Supplement of Atmos. Chem. Phys., 24, 3759–3768, 2024
https://doi.org/10.5194/acp-24-3759-2024-supplement
© Author(s) 2024. CC BY 4.0 License.

Atmospheric Chemistry and Physics
Open Access
EGU

Supplement of

Comment on "Transport of substantial stratospheric ozone to the surface by a dying typhoon and shallow convection" by Chen et al. (2022)

Xiangdong Zheng et al.

Correspondence to: Xiaobin Xu (xiaobin_xu@189.cn)

The copyright of individual parts of the supplement might differ from the article licence.

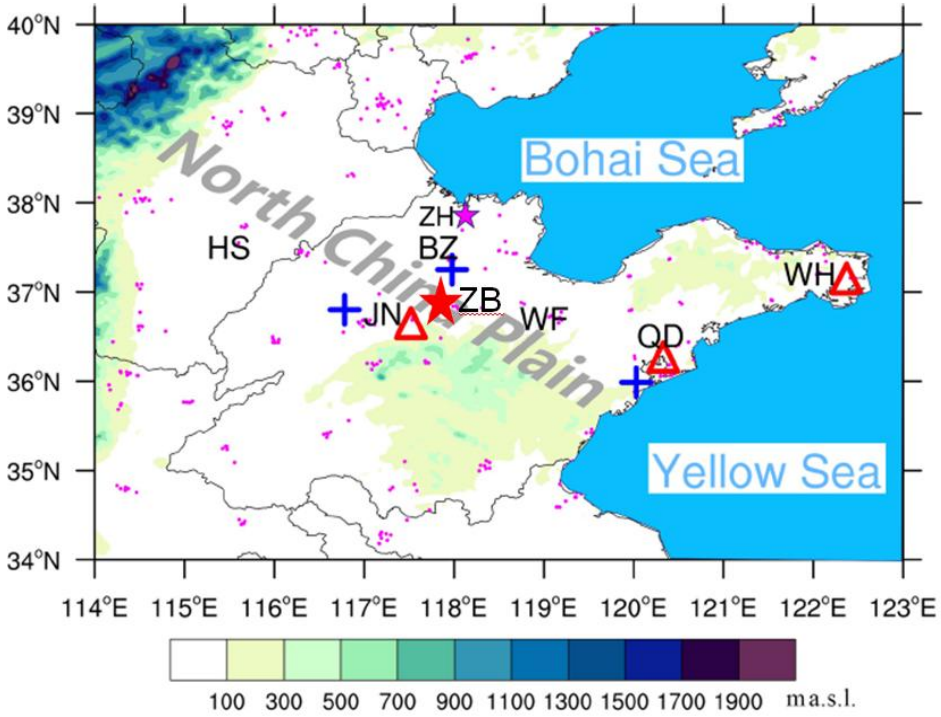

Figure S1: Map modified from Figure 1 in Chen et al. (2022) showing the NCP and its topography with locations of related cities Hengshui (HS), Jinan (JN), Binzhou (BZ), Weifang (WF), Qingdao (QD), Weihai (WH), and Zibo (ZB, red star, newly added in this study). ZB roughly occupies the area of 36.5 °-36.8 °N and 117.9 °-118.0 °E. Other details see Chen et al. (2022).

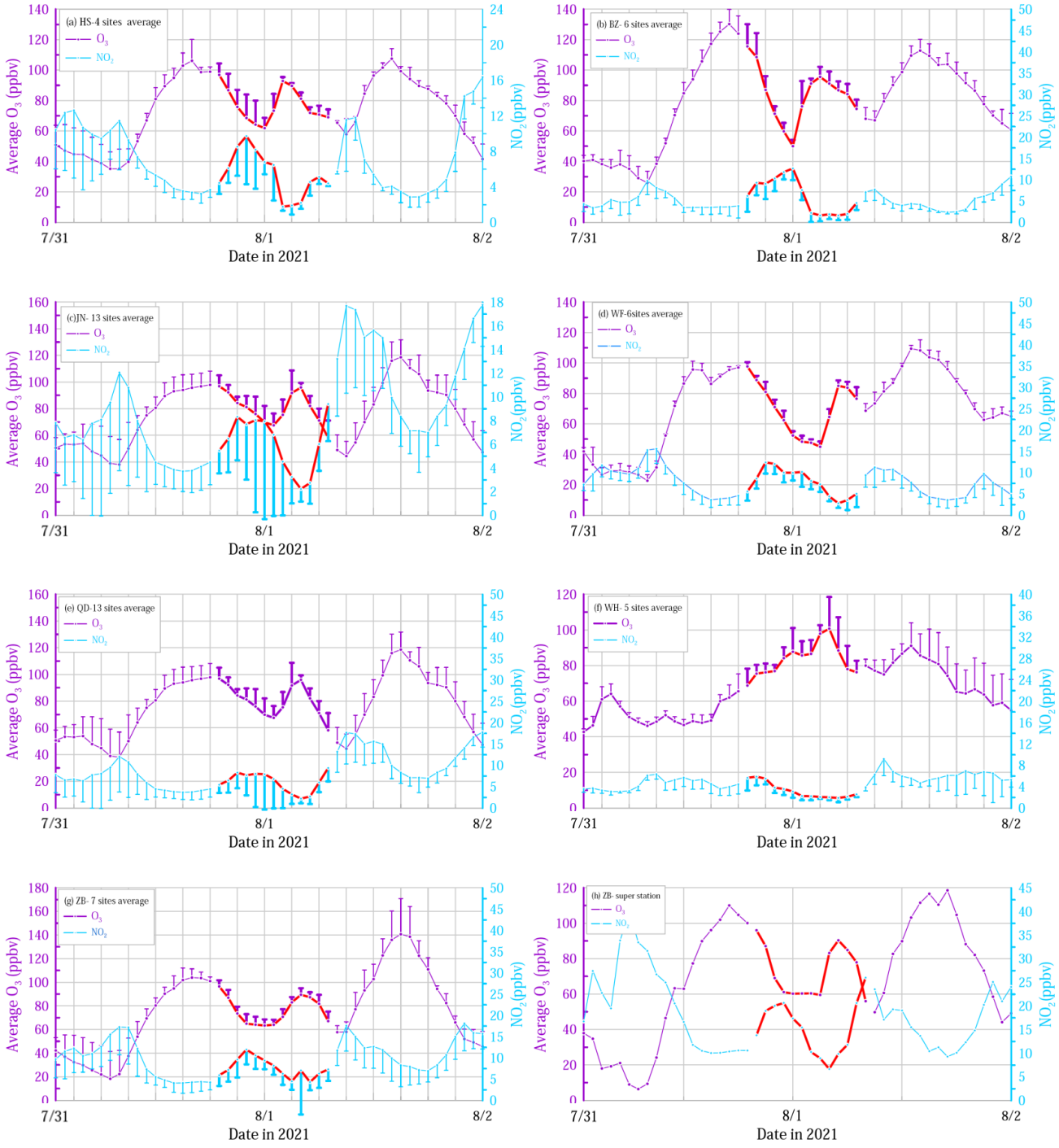

Figure S2. same as Figure 1 but showing only the period from 00:00 LT on 31 July to 23:00 LT on 1 August to highlight the NOEs. The error bars indicate 1 standard deviation of average O_3 (up) and NO_2 (down).

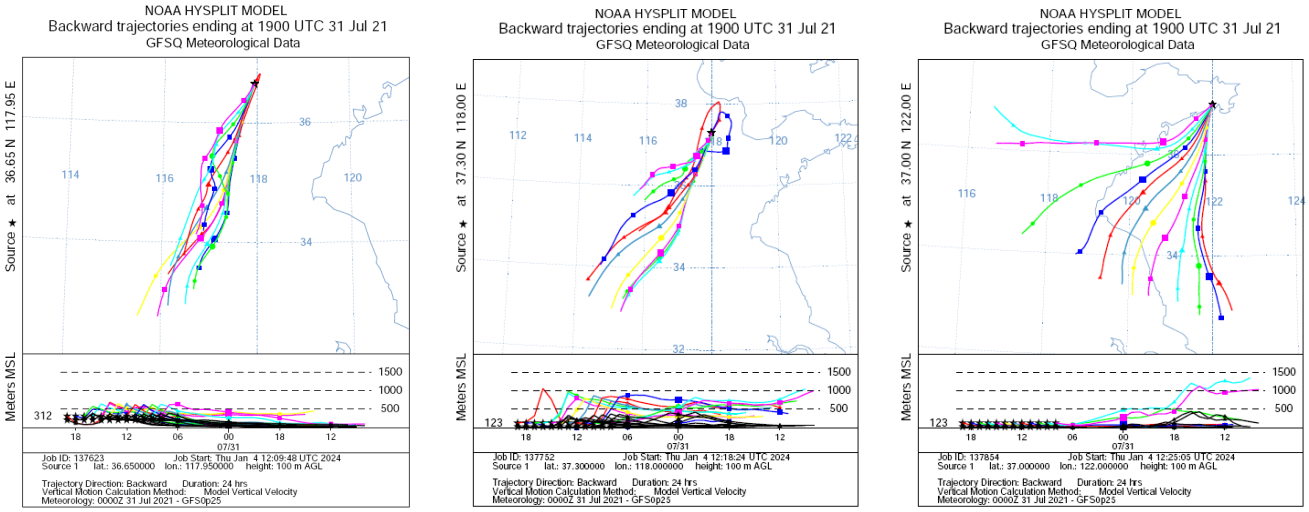

Figure S3. Backward trajectories for air parcels arriving at 100 m above ground over Zibo (ZB, left), Binzhou (BZ, middle) and Weihai (WH, right) every hour between 19:00 and 08:00 UTC, 31 July 2021. The trajectories were computed online using the HYSPLIT model (https://www.ready.noaa.gov/HYSPLIT.php; Stein et al. 2015; Rolph et al., 2017) and the Global Forecast System (GFS) reanalysis data (0.25 ° resolution, https://www.emc.ncep.noaa.gov/emc/pages/numerical_forecast_systems/gfs.php). The total run time for the trajectories was 24 hours.

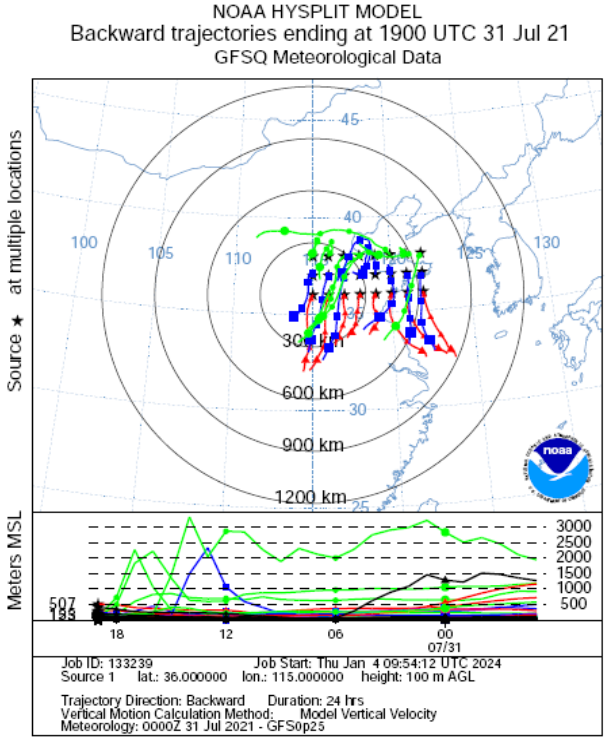

Figure S4. Matrix of backward trajectories for air parcels arriving at 100 m above ground over the domain 36 °-38 °N and 115 °-122 °E at 19:00 UTC, 31 July 2021. The trajectories were computed online using the HYSPLIT model (https://www.ready.noaa.gov/HYSPLIT.php; Stein et al. 2015; Rolph et al., 2017) and the Global Forecast System (GFS) reanalysis data (0.25 ° resolution, https://www.emc.ncep.noaa.gov/emc/pages/numerical_forecast_systems/gfs.php). The total run time for the trajectories was 24 hours.

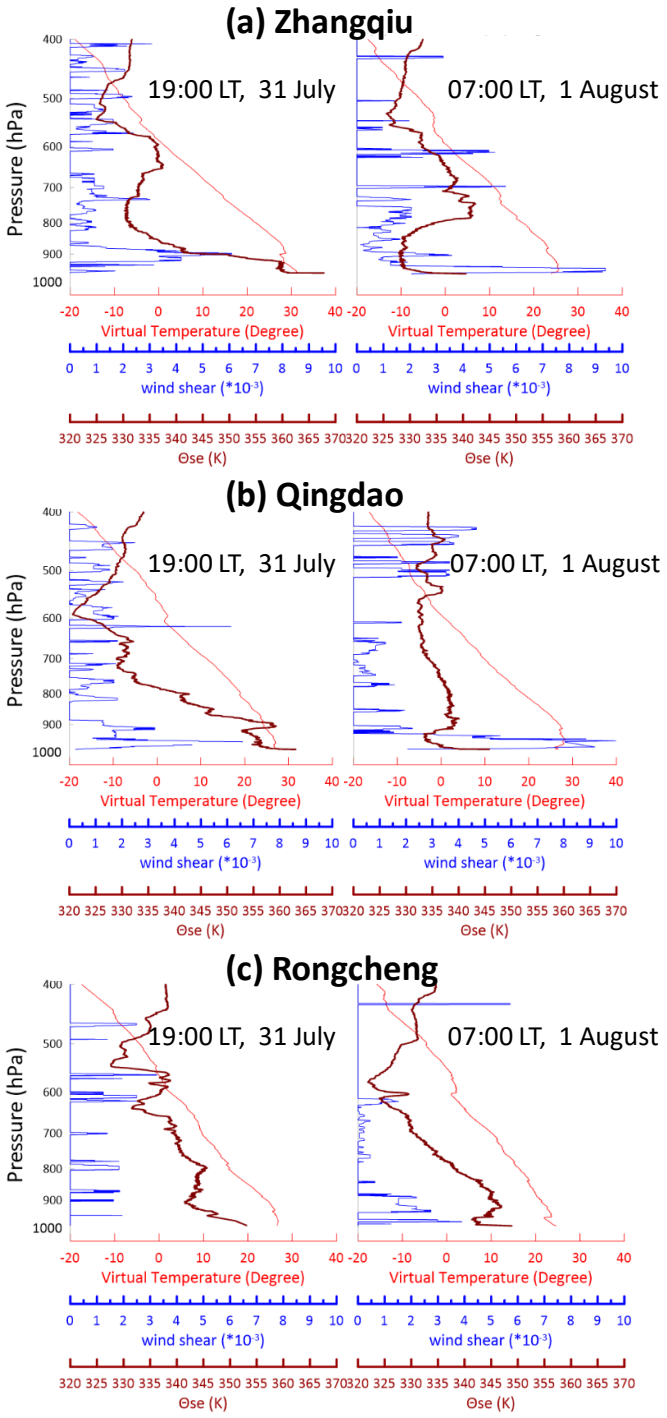

Figure S5. The vertical profiles of virtual temperature (red), equivalent potential temperature (θse, grey) and wind shear (blue) calculated on the basis of routine radiosonde observations data at 19:00 LT on 31 July and 07:00 LT on 1 August 2021 in Zhangqiu (ZQ)(a), Qingdao (QD)(b) and Rongcheng (RC) (c).

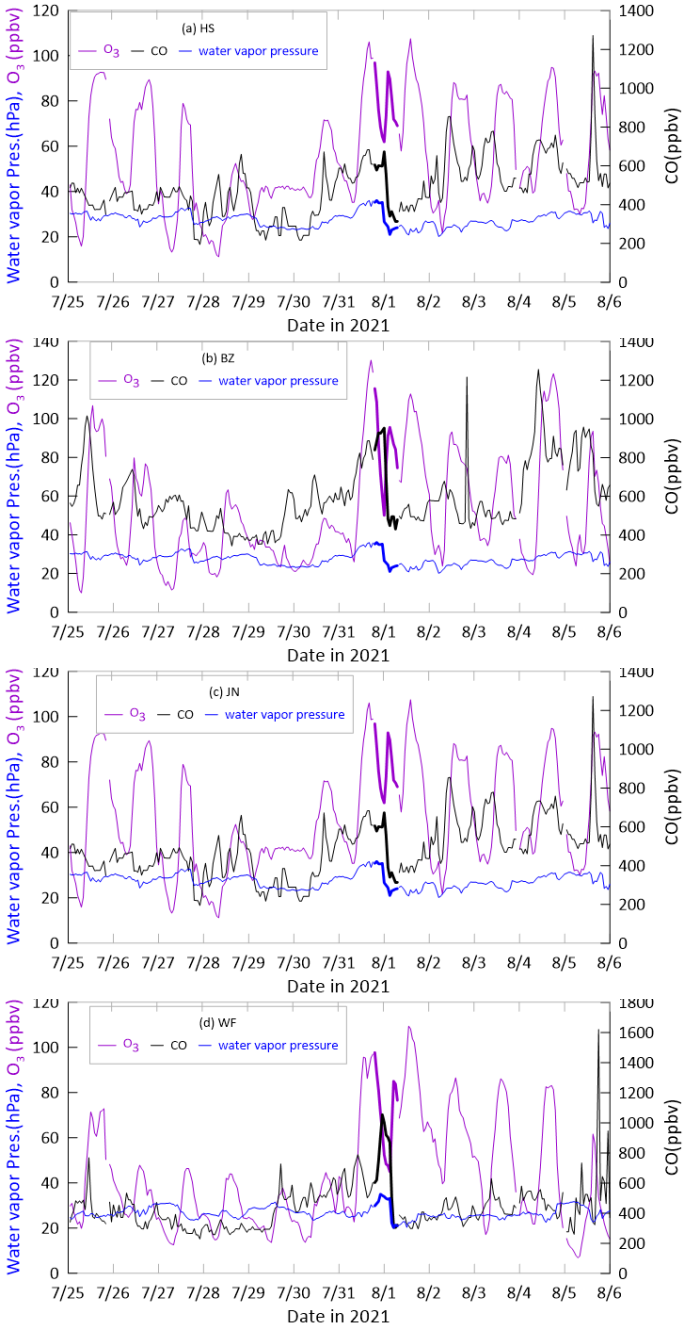

25 **Figure S6. Time series of hourly multi-sites-averages of O_3 (purple), CO (black) and water vapor pressure (blue) between 25 July and 5 August 2021. Data from 18:00 LT on 31 July to 06:00 LT on 1 August are highlighted in thick lines. The multi-site data from HS (4 sites) (a), BZ (6 sites) (b), JN (13 sites)(c), WF (6 sites) (d), QD (13 sites) (e),WH (5 sites)(f) and ZB (7sites) (g) are available at https://quotsoft.net/air (last access: 15 April 2023; X. L. Wang, 2020). Data from the ZB supersite (h) is provided by the Chinese Academy of Environmental Sciences (CRAES). Water vapor pressure data are from https://data.cma.cn/.**

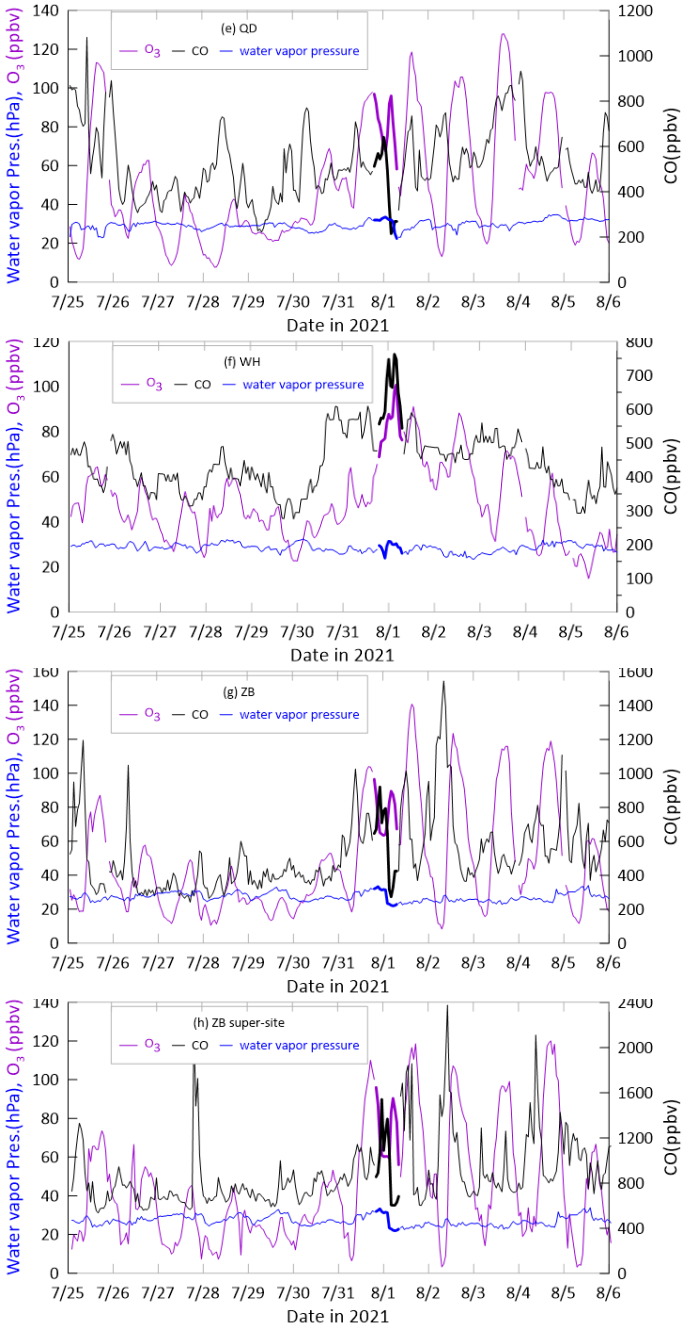

Figure S6. (continued).

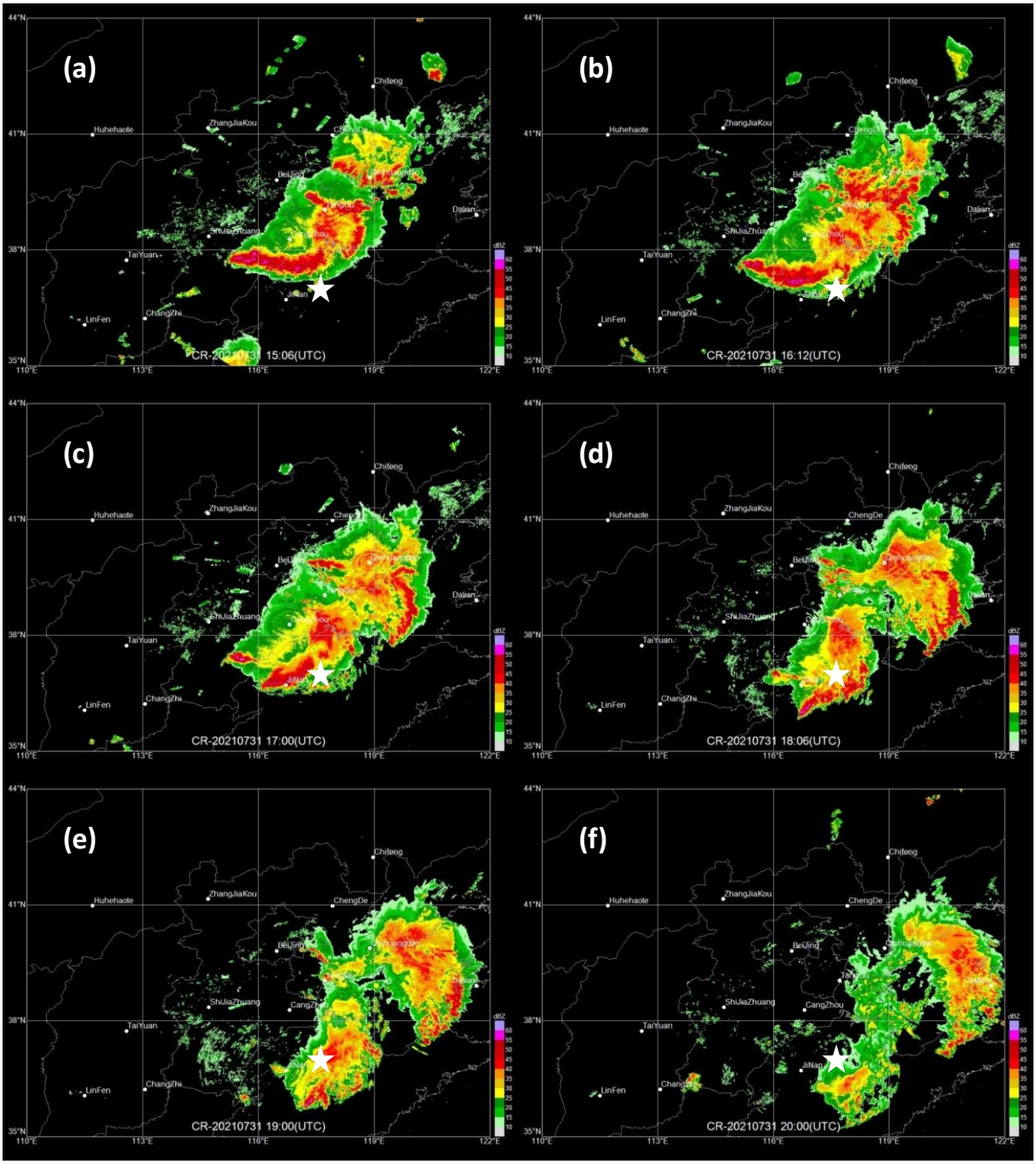

Figure S7. Radar reflectivity maps for the North China Plain at (a) 15:06 UTC (23:00 LT, 31 July), (b) 16:12 UTC (00:12 LT, 1 August), (c) 17:00 UTC (01:00 LT, 1 August), (d) 18:06 UTC (02:06 LT, 1 August), (e) 19:00 UTC (03:00 LT, 1 August) and (f) 20:00 UTC (04:00 LT, 1 August). Some of the major cities are indicated on the maps. The white star on each map shows the location of Zibo. The radar reflectivity maps were provided by Institute of Artificial Intelligence for Meteorology (IAIM), Chinese Academy of Meteorological Sciences (CAMS).

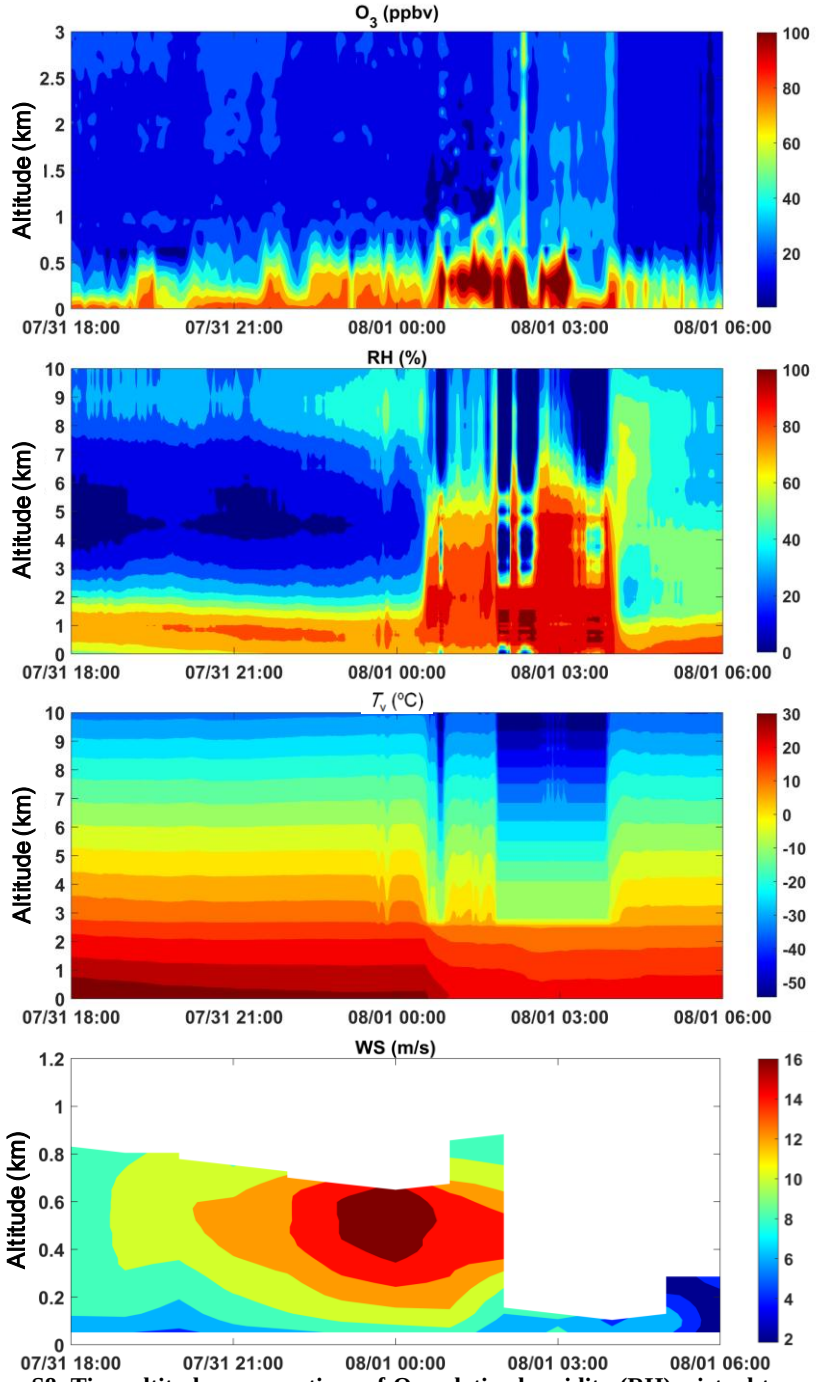

Figure S8. Time-altitude cross sections of O_3, relative humidity (RH), virtual temperature (T_v) and wind speed (WS) observed at the ZB supersite between 18:00 LT, 31 July and 06:00 LT, 1 August 2021. Vertical profiles of O_3 were obtained by a Lidar (RayOL-GB, Anhui Kechuang Zhongguang Technology Co., Ltd., China). Profiles of RH and Tv were detected by a microwave radiometer (KT-001, Qingdao Tianlang Environmental Technology Co., Ltd., China). Vertical distributions of WS were observed by a wind profiler radar (WindPrint V2000, Qingdao Huanhang Safety Environment Technology Co., Ltd, China).

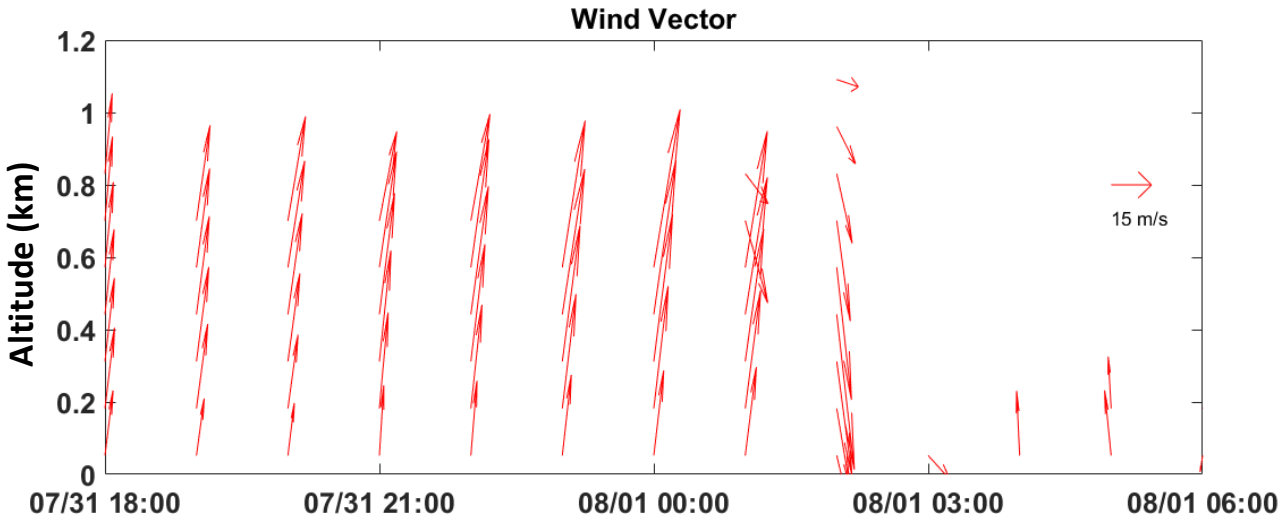

Figure S9. Hourly averaged wind vector below 1 km over the ZB supersite between 18:00 LT, 31 July and 06:00 LT, 1 August 2021. Wind data were observed by a wind profiler radar (WindPrint V2000, Qingdao Huanhang Safety Environment Technology Co., Ltd, China).

Section S1 Identifying potential origin of the NOE by comparing afternoon O_3 with O_x in the NBL during the NOE

Our intention is to check whether or not surface O_3 observed during the NOE contained significant contribution of O_3 from the stratosphere. For this purpose, a comparison of O_3 levels in the vertical direction is helpful. However, O_3 is very reactive and can be significantly removed by titration reactions in the boundary layer, with $O_3 + NO = NO_2 + O_2$ being the most important one. Therefore, O_x (O_3+NO_2) is a more conserved quantity than O_3 and hence a better metric for comparison (Kley et al., 1994; Kleinmann et al., 2002; Caputi et al., 2019; He et al., 2022). During daytime, NO_2 formed in the titration reaction is rapidly photolyzed to regenerate O_3 so that the net chemical loss of O_3 is relatively small. At night, however, the reaction between O_3 and NO leads to lower levels of O_3 in the nocturnal boundary layer (NBL) and in the residual layer (RL). Because the emission of NO takes place mainly in the NBL, much more O_3 is removed by the titration reaction in the NBL than in the RL (Wang et al., 2018; Caputi et al., 2019; He et al., 2022). In addition, O_3 in the NBL is subjected to dry deposition. Therefore, the O_3 level before sunset largely remains in the RL (Caputi et al., 2019; He et al., 2022) and is usually much higher in the RL than in the NBL under normal conditions.

Following the method of He et al. (2022), we make comparison of afternoon O_3 averages on 31 July with the respective O_x averages in the NBL during the NOE between 31 July and 1 August, 2021. To facilitate the comparison, we treat the average surface O_3 during 14:00-17:00 LT of 31 July as afternoon average of O_3 in the convective boundary layer, denoted as $[O_3]_{aft}$. Let us now focus on three nighttime atmospheric conditions, (I) undisturbed, (II) disturbed with NOE but no STT impact, and (III) disturbed with NOE and significant STT impact.

Under undisturbed condition (I), the nighttime average O_3 concentration in the RL ($[O_3]_{RL}$) should be close to (or only slightly lower than) $[O_3]_{aft}$ (Caputi et al., 2019; He et al., 2022), while the average O_3 concentration in the NBL ($[O_3]_{NBL}$)

should be much lower than $[O_3]_{aft}$ due to the impacts of NO titration ($\Delta[O_3]_{titr}$) and dry deposition ($\Delta[O_3]_{dep}$), and the average O_x concentration in the NBL ($[O_x]_{NBL}$) should also be lower than $[O_3]_{aft}$ due to dry deposition. The following relationships should be tenable:

$$[O_3]_{RL} \leq [O_3]_{aft} \quad (S1)$$

$$[O_3]_{NBL} = [O_3]_{aft} - \Delta[O_3]_{titr} - \Delta[O_3]_{dep} \quad (S2)$$

$$[O_x]_{NBL} = [O_3]_{aft} - \Delta[O_3]_{dep} \quad (S3)$$

Under disturbed condition with NOE but no STT impact (II), a downward transport of O_3 from the RL to NBL should be considered. Assuming that the downward transport causes a reduction of $[O_3]_{RL}$ by $\Delta[O_3]_{D1}$ and an increase of $[O_3]_{NBL}$ by $\Delta[O_3]_{D2}$, then

$$[O_3]_{RL} \leq [O_3]_{aft} - \Delta[O_3]_{D1} \quad (S4)$$

$$[O_3]_{NBL} = [O_3]_{aft} - \Delta[O_3]_{titr} - \Delta[O_3]_{dep} + \Delta[O_3]_{D2} \quad (S5)$$

$$[O_x]_{NBL} = [O_3]_{aft} - \Delta[O_3]_{dep} + \Delta[O_3]_{D2} \quad (S6)$$

Under disturbed condition with NOE and STT impact (III), net contributions of O_3 from the STT should be considered to the RL and the NBL. Assuming that the STT contribution increases $[O_3]_{RL}$ and $[O_3]_{NBL}$ by $\Delta[O_3]_{STT1}$ and $\Delta[O_3]_{STT2}$, respectively, then

$$[O_3]_{RL} \leq [O_3]_{aft} + \Delta[O_3]_{STT1} \quad (S7)$$

$$[O_3]_{NBL} = [O_3]_{aft} - \Delta[O_3]_{titr} - \Delta[O_3]_{dep} + \Delta[O_3]_{STT2} \quad (S8)$$

$$[O_x]_{NBL} = [O_3]_{aft} - \Delta[O_3]_{dep} + \Delta[O_3]_{STT2} \quad (S9)$$

Equation (S3) indicates that $[O_x]_{NBL}$ should be significantly lower than $[O_3]_{aft}$ under undisturbed conditions. Although equation (S6) shows that $[O_x]_{NBL}$ could be higher than $[O_3]_{aft}$ (i.e., if $\Delta[O_3]_{dep} < \Delta[O_3]_{D2}$), it cannot really occur because $[O_3]_{RL} < [O_3]_{aft}$ (see equation (S4)) and O_3 cannot be transported from a lower concentration position to the higher one. Therefore, $[O_x]_{NBL}$ should not be significantly higher than $[O_3]_{aft}$ under disturbed conditions with NOE but no STT impact. Dry deposition is only a small sink for nighttime surface O_3 in northern China (Tang et al., 2017), while a STT impact could substantially enhanced the level of surface O_3 if it reaches the surface layer. Hence, it is very likely according to equation (S9) that $[O_x]_{NBL}$ is significantly higher than $[O_3]_{aft}$ under disturbed condition with a STT impact. In summary, $[O_x]_{NBL}$ should be significantly higher than $[O_3]_{aft}$ if the NBL is really impacted by stratospheric O_3, otherwise the STT impact is negligible even though a NOE event is observed.

Section S2. Estimating photochemical ages of air masses arrived at the Zibo supersite

Once emitted into the atmosphere, all hydrocarbons experience decay caused mainly by the oxidation of OH radical and atmospheric mixing (McKeen et a., 1990; Parrish et al., 1992). The relative compositions of hydrocarbons were used to study the histories of air masses over rural areas (Roberts et al., 1984) and remote marine areas (Rudolph et al., 1990). The so-called photochemical ages of air masses can be derived from observed ratios of hydrocarbons and OH mixing ratios either

measured or estimated. However, the calculated photochemical ages may be significantly impacted by atmospheric mixing on the ratios during transport (McKeen and Liu, 1993). Nevertheless, the estimation of photochemical age based on hydrocarbon ratios in air masses has been a current practice in atmospheric researches (e.g., Kleinman et al., 2003; Irei et al., 2016). Here, we follow the practice to estimate photochemical ages of air masses arrived at the Zibo (ZB) supersite during the NOE reported in Chen et al. (2022) and a few days before and after.

Hourly measurements of hydrocarbons at the supersite between 25 July and 5 August 2021 were used to calculated hydrocarbon ratios. Good correlations were found among some of the hydrocarbon ratios. Among the alkanes ratios, the best correlation existed between Ln(Butane/Ethane) and Ln(Propane/Ethane), with R^2=0.63 (Figure S10). Among the aromatics ratios, the best correlation existed between Ln(o-Xylene/Benzene) and Ln(Ethylbenzne/Benzene), with R^2=0.89 (Figure S11). In addition, there were also excellent correlations between Ln[Butane] and Ln[Propane] (R^2=0.78, Figure S12) and between Ln[o-Xylene] and Ln[Ethylbenzne] (R^2=0.85, Figure S13). These results indicate that ethane, propane and n-butane observed the supersite were very likely from the same sources and so were benzene, ethylbenzene and o-Xylene. Therefore, it is proper to estimate photochemical ages using the ratios between these alkanes and aromatics. We derived photochemical ages from the ratios [Butane]/[Propane] and [o-Xylene]/[Ethylbenzene].

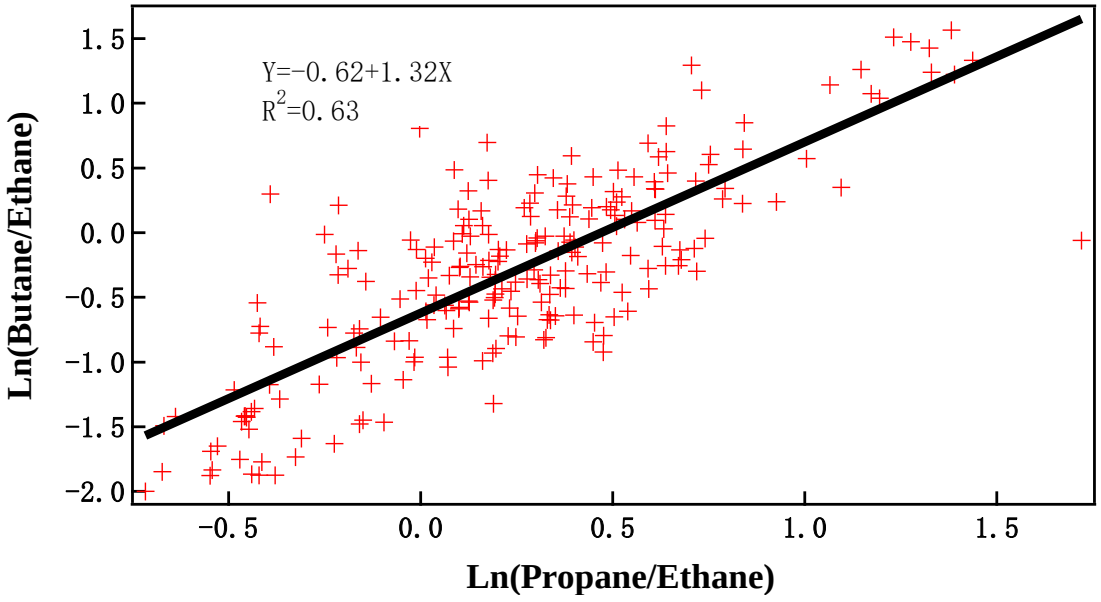

Figure S10: Correlation between Ln(Butane/Ethane) and Ln(Propane/Ethane).

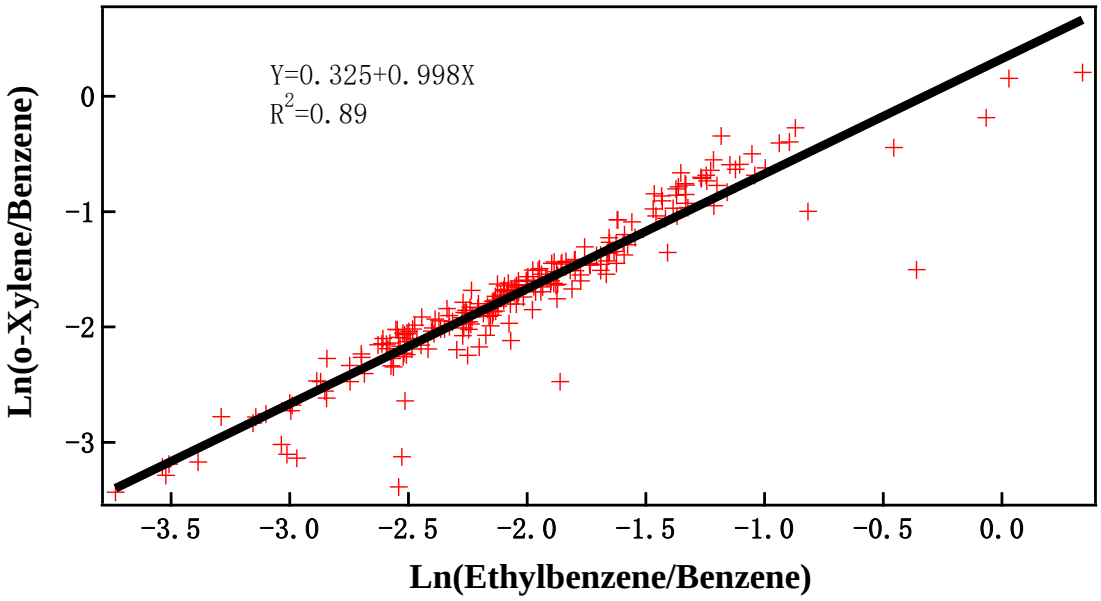

120

Figure S11: Correlation between Ln(o-Xylene/Benzene) and Ln(Ethylbenzne/Benzene).

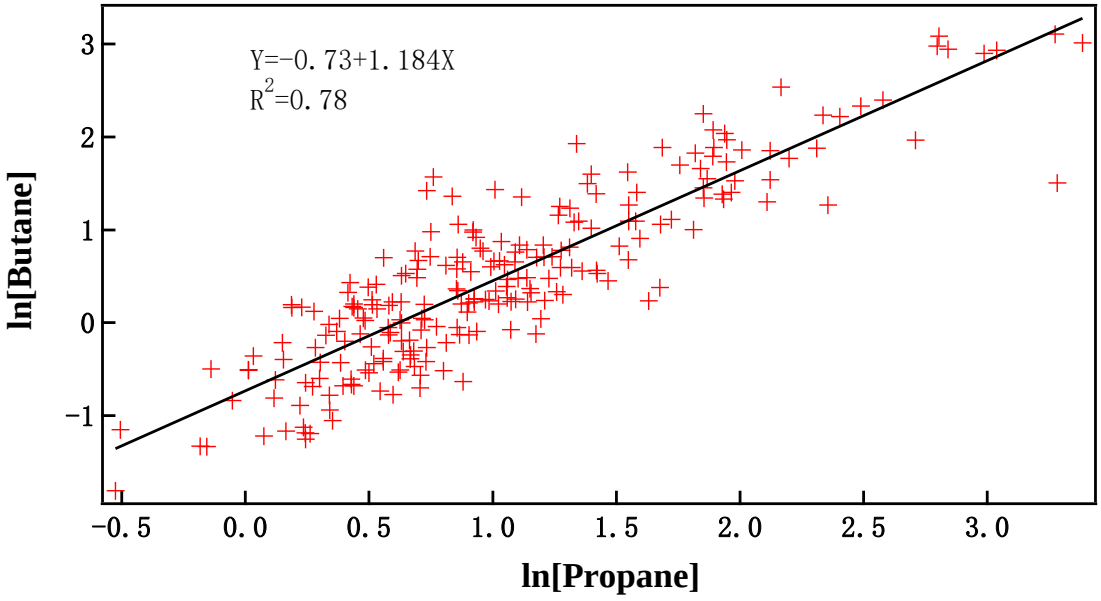

Figure S12: Correlation between butane and propane concentrations.

125

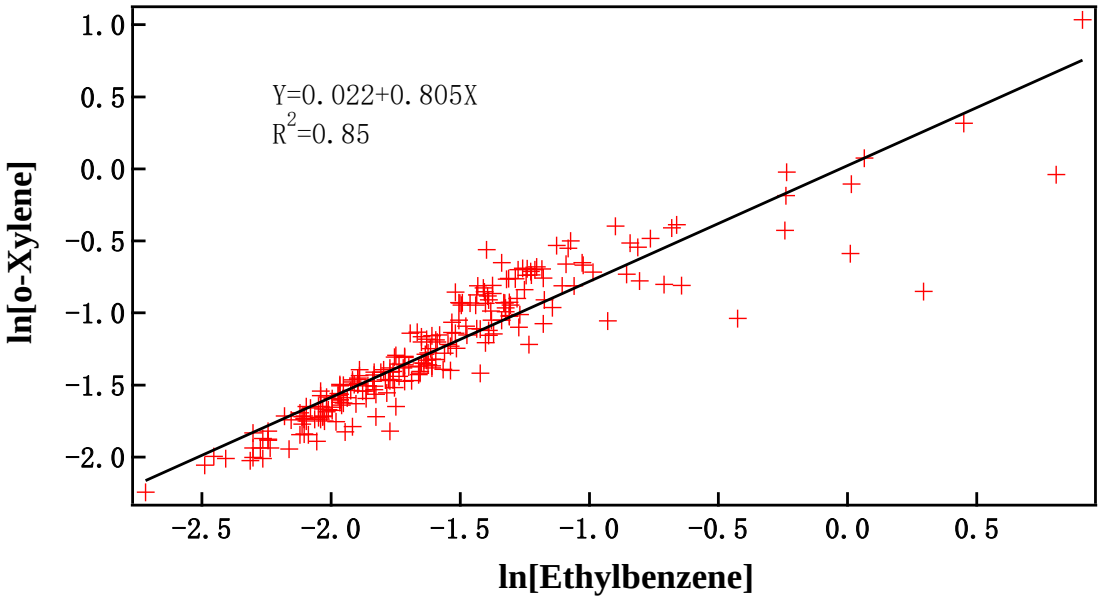

Figure S13: Correlation between o-xylenen and ethylbenzene concentrations.

Since the concentration of hydrocarbon X is enhanced by emissions and lowered by reaction with OH and mixing with background air, the change of the X concentration with time can be generally expressed as:

$$\frac{d[X]}{dt} = S_x - k_x[OH][X], \quad \text{(S10)}$$

where, [X] is the concentration of X; S_x represents collective impact on [X] of physical processes such as emissions, dilution, etc.; [OH] indicates the OH concentration averaged over the transport way; k_x is the rate constant for the X+OH reaction. Similar expression can be given for hydrocarbon Y:

$$\frac{d[Y]}{dt} = S_y - k_y[OH][Y]. \quad \text{(S11)}$$

In Eq. S10 and Eq. S11, S_x and S_y are unknown and difficult to obtain. However, their impacts on hydrocarbon concentrations are assumed to be low if the hydrocarbons are relatively reactive. After ignoring S_x and S_y in Eq. S10 and Eq. S11, the following equations can be obtained by integration from time 0 to t:

$$\ln [X] = \ln[X_0] - k_x[OH]t \quad \text{(S12)}$$

and

$$\ln [Y] = \ln[Y_0] - k_y[OH]t, \quad \text{(S13)}$$

with X_0 and Y_0 being the respective concentrations of X and Y initial after emissions.

Finally, a formula for calculating photochemical ages can be derived from Eq.S12 and Eq. S13:

$$t = \frac{1}{(k_y - k_x)[OH]} \cdot \left(\ln \frac{[Y_0]}{[X_0]} - \ln \frac{[Y]}{[X]}\right). \quad \text{(S14)}$$

Rate constants (k_x and k_y) are available in literature. Table S1. lists the rate constants at 298K for the reactions of OH with n-butane, propane, ethylbenzene and o-xylene. These rate constants were used in the estimation of photochemical ages without considering the influences of atmospheric conditions.

Table S1: Rate constants of the reactions of the OH radical with some hydrocarbons at 298K

Reaction	Rate constant, cm^3/mol/s	Reference
n-butane + OH	1.45×10^{12}	Talukdar et al. (1994)
Propane + OH	6.58×10^{11}	DeMore et al. (1997)
ethylbenzene + OH	4.52×10^{12}	Atkinson (1986)
o-xylene + OH	8.85×10^{12}	Atkinson (1986)

There was no observation of OH radical over ZB and surroundings. An assumption had to be made for the value of [OH] in Eq. S14. A recent study shows that the diel-average tropospheric column mean OH concentrations over the Yellow Sea and East China Sea areas were in the range of $(1.5\text{-}3)\times10^6$ molecules/cm^3 during July-August 2016 (Thompson et al., 2022). In-situ observations of vertical profiles of OH showed that the OH mixing ratio for 29 April 1994 varied roughly in the range of 0.2-0.4 pptv (about $(5\text{-}10)\times10^6$ molecules/cm^3) at the altitudes from 1 km to 12 km over Oklahoma, USA, with no consistent gradients (Brune et al., 1998). Ground measurements in summer of 2014 at Wangdu, a rural site in the North China Plain, showed median values of OH varying from 5×10^5 molecules/cm^3 at night to 6.8×10^6 molecules/cm^3 during 12:00-16:00 LT (Tan et al., 2017). Earlier observations made in August 2006 at Yufa, a suburban site in Beijing, showed the OH level varying from 6×10^5 molecules/cm^3 (detection limit) at night to $(4\text{-}17)\times10^6$ molecules/cm^3 around noontime (Lu et al., 2013). Given these data of OH values, we assumed the average value of OH over ZB and surroundings for the period in consideration (i.e., 25 July - 5 August 2021) to be 5×10^6 molecules/cm^3.

To obtain a better estimate of the range of photochemical ages, we calculated photochemical ages using both [Butane]/[Propane] and [o-Xylene]/[Ethylbenzene]. The initial values of [Butane]/[Propane] and [o-Xylene]/[Ethylbenzene] were not available. Therefore, we substituted the maximum [Butane]/[Propane] (2.25) and [o-Xylene]/[Ethylbenzene] (2.31) for the initial values of [Butane]/[Propane] and [o-Xylene]/[Ethylbenzene], respectively. These maximum ratios should be lower than the initial ones because they represented ratios certain time after the hydrocarbons were emitted. This may more or less underestimate photochemical ages but does not change our conclusion.

The photochemical ages of air masses arrived at the ZB supersite during 25 July – 5 August 2021 were calculated using Eq. S14, and based on [Butane]/[Propane] and [o-Xylene]/[Ethylbenzene], respectively. The two sets of estimated photochemical ages are shown in Figure 3, together with the observed O_3 data.

References

Atkinson, R.: Kinetics and mechanisms of the gas-phase reactions of the hydroxyl radical with organic compounds under atmospheric conditions, Chem. Rev., 86, 69,1986.

Brune, W.H., Faloona, I.C., Tan, D., Weinheimer, A.J., Campos, T., Ridley, B.A., Vay, S.A., Collins, J.E., Sachse, G.W., Jaegle, L., and Jacob, D.J.: Airborne in-situ OH and HO_2 observations in the cloud-free troposphere and lower stratosphere during SUCCESS, Geophys. Res. Lett., 25(10), 1701-1704, 1998.

Caputi, D.J., Faloona, I., Trousdell, J., Smoot, J., Falk, N., and Conley, S.: Residual layer ozone, mixing, and the nocturnal jet in California's San Joaquin Valley, Atmos. Chem. Phys., 19, 4721–4740, https://doi.org/10.5194/acp-19-4721-2019, 2019.

Chen, Z., Liu, J., Qie, X., Cheng, X., Shen, Y., Yang, M., Jiang, R., and Liu., X.: Transport of substantial stratospheric ozone to the surface by a dying typhoon and shallow convection, Atmos. Chem. Phys., 22, 8221–8240, https://doi.org/10.5194/acp-22-8221-2022, 2022.

DeMore, W.B., Sander, S.P., Golden, D.M., Hampson, R.F., Kurylo, M.J., Howard, C.J., Ravishankara, A.R., Kolb, C.E., and Molina, M.J.: Chemical kinetics and photochemical data for use in stratospheric modeling. Evaluation number 12, JPL Publication, 97-4 , 1-266, 1997.

He, C., Lu, X., Wang, H., Wang, H., Li, Y., He, G., He, Y., Wang, Y., Zhang, Y., Liu, Y., Fan, Q., and Fan, S.: The unexpected high frequency of nocturnal surface ozone enhancement events over China: characteristics and mechanisms, Atmos. Chem. Phys., 22, 15243–15261, https://doi.org/10.5194/acp-22-15243-2022, 2022.

Irei, S., Takami, A., Sadanaga, Y., Nozoe, S., Yonemura, S., Bandow, H., and Yokouchi, Y.: Photochemical age of air pollutants, ozone, and secondary organic aerosol in transboundary air observed on Fukue Island, Nagasaki, Japan, Atmos. Chem. Phys., 16, 4555–4568, https://doi.org/10.5194/acp-16-4555-2016, 2016.

Kleinman, L.I., Daum, P.H., Lee, Y.-N., Nunnermacher, L.J., Springston, S.R., Weinstein-Lloydm J., Hyde, P., Doskey, P., Rudolph, J., Fst, J., and Berkowizt, C.: Photochemical age determinations in the Phoenix metropolitan area, J. Geophys. Res., 108(D3), 4096, doi:10.1029/2002JD002621, 2003.

Lu, K. D., Hofzumahaus, A., Holland, F., Bohn, B., Brauers, T., Fuchs, H., Hu, M., Häseler, R., Kita, K., Kondo, Y., Li, X., Lou, S. R., Oebel, A., Shao, M., Zeng, L. M., Wahner, A., Zhu, T., Zhang, Y. H., and Rohrer, F.: Missing OH source in a suburban environment near Beijing: observed and modelled OH and HO_2 concentrations in summer 2006, Atmos. Chem. Phys., 13, 1057–1080, https://doi.org/10.5194/acp-13-1057-2013, 2013.

McKeen, S.A., and Liu, S.C.: Hydrocarbon ratios and photochemical history of air masses, Geophys. Res. Lett., 20, 2363-2366, 1993.

McKeen, S.A., Trainer, M, E.Y. Hsie, R.K. Tallamraju, and S.C.Liu, On the indirect determination of atmospheric OH radical concentrations from reactive hydrocarbon measurements, J. Geophys. Res., 95, 7493-7500, 1990.

Parrish, D.D., Hahn, C.J., Williams, E.J., Norton, R.B., Fehsenfeld, F.C., Singh, H.B., Shetter, J.D., Gandrun, B.W., and Ridley, B.A.: Indications of photochemical histories of pacific air masses from measurements of atmospheric trace species at Point Arena, Califonia, J. Geophys. Res., 97, 15883-15902, 1992.

Rolph, G., Stein, A., and Stunder, B.: Real-time Environmental Applications and Display sYstem: READY. Environmental Modelling & Software, 95, 210-228, https://doi.org/10.1016/j.envsoft.2017.06.025, 2017.

Roberts, J.M., Fehsenfeld, F.C., Liu, S.C., Bollinger, M.J., Hahn, C., Albritton, D.L., and Sievers, R.E.: Measurements of aromatic hydrocarbon ratios and NO_x concentrations in the rural troposphere: Observation of air mass photochemical aging and NO_x removal, Atmos. Environ., 18, 2421-2432, 1984.

Rudolph, J., and Johnen, FJ： Measurements of light atmospheric hydrocarbons over the Atlantic in regions of low biological activity, J. Geophys. Res., 95, 20583-20591, 1990.

Stein, A.F., Draxler, R.R, Rolph, G.D., Stunder, B.J.B., Cohen, M.D., and Ngan, F.: NOAA's HYSPLIT atmospheric transport and dispersion modeling system, Bull. Amer. Meteor. Soc., 96, 2059-2077, http://dx.doi.org/10.1175/BAMS-D-14-00110.1., 2015.

Talukdar, R.K., Melouki, A., Gierczak, T., Barone, S., Chiang, S-Y., and Ravishankara, A.R.: Kinetics of the reactions of OH with alkanes, Int. J. Chem. Kinet., 26, 973-990, 1994.

Tan, Z., Fuchs, H., Lu, K., Hofzumahaus, A., Bohn, B., Broch, S., Dong, H., Gomm, S., Häseler, R., He, L., Holland, F., Li, X., Liu, Y., Lu, S., Rohrer, F., Shao, M., Wang, B., Wang, M., Wu, Y., Zeng, L., Zhang, Y., Wahner, A., and Zhang, Y.: Radical chemistry at a rural site (Wangdu) in the North China Plain: observation and model calculations of OH, HO_2 and RO_2 radicals, Atmos. Chem. Phys., 17, 663–690, https://doi.org/10.5194/acp-17-663-2017, 2017.

Thompson, C.R., Wofsy, S.C., Prather, M.J., Newman, P.A., Hanisco, T.F., Ryerson, T.B., Fahey, D.W., Apel, E.C., Brock, C.A., Brune, W.H., Froyd, K., Katich, J.M., Nicely, J.M., Peischl, J., Ray, E., Veres, P.R., Wang, S., Allen, H.M., Asher, E., Bian, H., Blake, D., Bourgeois, I., Budney, J., Bui, T.P., Butler, A., Campuzano-Jost, P., Chang, C., Chin, M., Commane, R., Correa, G., Crounse, J.D., Daube, B., Dibb, J.E., DiGangi, J.P., Diskin, G.S., Dollner, M., Elkins, J.W., Fiore, A.M., Flynn, C.M., Guo, H., Hall, S.R., Hannun, R.A., Hills, A., Hintsa, E.C., Hodzic, A., Hornbrook, R.S., Huey, L.G., Jimenez, J.L., Keeling, R.F., Kim, M.J., Kupc, A., Lacey, F., Lait, L.R., Lamarque, J.-F., Liu, J., McKain, K., Meinardi, S., Miller, D.O., Montzka, S.A., Moore, F.L., Morgan, E.J., Murphy, D.M., Murray, L.T., Nault, B.A., Neuman, J.N., Nguyen, L., Gonzalez, Y., Rollins, A., Rosenlof, K., Sargent, M., Schill, G., Schwarz, J.P., St. Clair, J.M., Steenrod, S.D., Stephens, B.B., Strahan, S.E., Strode, S.A., Sweeney, C., Thames, A.B., Ullmann, K., Wagner, N., Weber, R., Weinzierl, B., Wennberg, P.O., Williamson, C.J., Wolfe, G.M., and Zeng, L.: The NASA Atmospheric Tomography (ATom) Mission Imaging the Chemistry of the Global Atmosphere, Bulletin of American Meteorological Society, E761-790, https://doi.org/10.1175/BAMS-D-20-0315.1, 2022.

Wang, H., Lu, K., Chen, X., Zhu, Q., Wu, Z., Wu, Y., and Sun, K.: Fast particulate nitrate formation via N_2O_5 uptake aloft in winter in Beijing, Atmos. Chem. Phys., 18, 10483–10495, https://doi.org/10.5194/acp-18-10483-2018, 2018.